A Deep ALMA Image of the Hubble Ultra Deep Field

James S. Dunlop[1]

[1] Institute for Astronomy, University of Edinburgh, UK

Although primarily designed as a high-resolution imaging spectrometer at sub-millimetre/millimetre wavelengths, the Atacama Large Millimeter/submillimeter Array (ALMA) has a vital role to play in producing the key deep, unconfused, submillimetre/millimetre continuum surveys required to bridge the current gap in our understanding of visible and dust-obscured star formation in the young Universe. The first such survey has now been completed, comprising a mosaic of 45 ALMA pointings at a wavelength of 1.3 mm, covering the Hubble Ultra Deep Field (HUDF). This deep, homogeneous ALMA survey, combined with the wealth of existing data in the HUDF, has already provided new clarity on the nature of dusty star-forming galaxies, and the relative evolution of dust-obscured and unobscured star formation over cosmic time.

Team members:
J. S. Dunlop[1], R. J. McLure[1], A. D. Biggs[2], J. E. Geach[3], M. J. Michalowski[1], R. J. Ivison[1,2], W. Rujopakarn[4], E. van Kampen[2], A. Kirkpatrick[5], A. Pope[5], D. Scott[6], A. M. Swinbank[7], T. A. Targett[8], I. Aretxaga[9], J. E. Austermann[10], P. N. Best[1], V. A. Bruce[1], E. L. Chapin[11], S. Charlot[12], M. Cirasuolo[2], K. Coppin[3], R. S. Ellis[2], S. L. Finkelstein[13], C. Hayward[14], D. H. Hughes[9], E. Ibar[15], P. Jagannathan[16], S. Khochfar[1], M. P. Koprowski[3], D. Narayanan[17], K. Nyland[18], C. Papovich[19], J. A. Peacock[1], G. H. Rieke[20], B. Robertson[21], T. Vernstrom[22], P. P. van der Werf[23], G. W. Wilson[5], M. Yun[5]

[1] Institute for Astronomy, University of Edinburgh, UK; [2] ESO; [3] Centre for Astrophysics Research, University of Hertfordshire, UK; [4] Department of Physics, Chulalongkorn University, Thailand; [5] Department of Astronomy, University of Massachusetts, USA; [6] Department of Physics and Astronomy, University of British Columbia, Canada; [7] Centre for Extragalactic Astronomy, Durham University, UK; [8] Department of Physics and Astronomy, Sonoma State University, USA; [9] Instituto Nacional de Astrofisica, Óptica y Electrónica (INAOE), Mexico; [10] NIST Quantum Devices Group, Boulder, USA; [11] Herzberg Astronomy and Astrophysics, National Research Council Canada, Victoria, Canada; [12] Sorbonne Universités, UPMC-CNRS, UMR7095, Institut d'Astrophysique de Paris, France; [13] Department of Astronomy, The University of Texas at Austin, Austin, USA; [14] California Institute of Technology, Pasadena, USA; [15] Instituto de Física y Astronomía, Universidad de Valparaíso, Chile; [16] National Radio Astronomy Observatory, Socorro, USA; [17] Department of Physics and Astronomy, Haverford College, USA; [18] National Radio Astronomy Observatory, Charlottesville, USA; [19] Department of Physics and Astronomy, Texas A. & M. University, USA; [20] Steward Observatory, University of Arizona, USA; [21] Department of Astronomy and Astrophysics, University of California, Santa Cruz, USA; [22] Dunlap Institute for Astronomy and Astrophysics, University of Toronto, Canada; [23] Leiden Observatory, Leiden University, the Netherlands.

Background: the importance of ALMA as a survey instrument

The Atacama Large Millimeter/submillimeter Array (ALMA) on the high Chajnantor plateau is now delivering on its promise to revolutionise astronomy and astrophysics in the challenging wavelength regime between ~ 0.3 mm and ~ 3 mm. Since the Earth's atmosphere is both a strong emitter and absorber of submillimetre radiation, observations at these wavelengths would ideally be conducted from outer space. However, creating submillimetre/millimetre (sub-mm/mm) images with an angular resolution comparable to the best optical images, as delivered, for example, by the Hubble Space Telescope (HST), requires a telescope aperture hundreds of times larger than can currently be launched into space. Indeed it requires a telescope aperture much larger than any single-dish telescope ever constructed on the ground. However, through the technique of aperture synthesis, the signals from many moderate-size telescope dishes can be combined to mimic the imaging capability of a single enormous telescope. Thus ALMA, with 66 moveable dishes, located above much of the atmosphere at an altitude of 5050 m, represents humanity's current best effort to realise the potential benefits of a giant sub-mm/mm telescope in space.

One might reasonably ask why so much effort and finance have been invested in creating what is currently the world's largest astronomical project. One answer, at least from the perspective of extra-galactic astronomy, is that approximately half of the optical/ultraviolet starlight emitted over cosmic history has been absorbed and then re-emitted at infrared-millimetre wavelengths by cosmic dust. Thus, a complete history of star and galaxy formation/evolution requires observations at both optical and far-infrared wavelengths, and the expansion of the Universe means that the dust emission from early/distant galaxies is redshifted from the far-infrared into the sub-mm/mm regime.

The importance of dust emission from galaxies became clear towards the end of the 20th century, first through the discoveries of the Infra-Red Astronomical Satellite (IRAS), and then with the advent of sub-mm imaging on large ground-based single-dish telescopes, such as the 15-metre diameter James Clerk Maxwell Telescope (JCMT) in Hawaii. The first deep blank-field sub-mm surveys of the sky, undertaken with the Submillimetre Common-User Bolometer Array (SCUBA) camera on the JCMT, revealed a population of distant galaxies which were almost completely dust-obscured, and whose far-infrared luminosities implied star formation rates of ~ 1000 $M_{\odot}$ yr^{-1} (for example, Hughes et al., 1998). In the intervening years the prevalence/importance of extreme dusty star-forming galaxies in the young Universe has been confirmed through surveys with the Submillimetre Common-User Bolometer Array (SCUBA), the Astronomical Thermal Emission Camera (AzTEC), and now SCUBA-2, all on the JCMT, with the Large APEX BOlometer Camera (LABOCA) on the Atacama Pathfinder EXperiment (APEX) telescope, and with the Herschel Space Observatory (for example, Coppin et al., 2006; Weiss et al., 2009; Burgarella et al., 2013; Michalowski et al., 2016).

Despite these impressive advances, with a maximum aperture diameter of 15 metres, these single-dish facilities have only been able to deliver sub-mm/mm imaging of very modest quality (for example, in the case of the JCMT, imaging with a full width half maximum [FWHM] of 14.5 arcseconds at wavelength ~ 850 μm). This unavoidable technical/physical limitation has two serious consequences. First, distant galaxies appear as unresolved blobs, with somewhat uncertain positions, making accurate comparison with optical imaging extremely problematic. Second, the large image size means that the achievable imaging depth is limited not by integration time, but by source confusion, where the blurred images of fainter galaxies ultimately overlap, forming an impenetrable background against which the brightness of only the most luminous rare sources

can be measured with acceptable accuracy. As a consequence, our sub-mm/mm view of the distant Universe has remained somewhat disconnected from our optical/near-infrared view.

While deep HST surveys are sensitive to faint galaxies with (unobscured) star formation rates smaller than 1 $M_{\odot}$ yr^{-1}, single-dish sub-mm/mm surveys have only really been effective at uncovering rare, extreme star-forming galaxies with dust-obscured star formation rates of several hundred $M_{\odot}$ yr^{-1}. While the latter objects present an interesting and important challenge to theoretical models of galaxy formation (for example, Narayanan et al., 2015), they provide only ~ 10 % of the measured far-infrared/mm background, and attempts to complete our inventory of dust-obscured star formation have had to rely on stacking experiments (for example, Geach et al., 2013; Bourne et al., 2016).

Since its individual 12-metre diameter dishes can be driven to separations of several kilometres, ALMA is more than capable of transforming this situation: it can deliver angular resolutions of a few milli-arcseconds and also high-resolution spectroscopy at sub-mm/mm wavelengths. However, from the perspective of survey astronomy, this stunning resolution comes at a price. First, because ALMA is an interferometer (rather than a single telescope and multi-pixel camera) the angular field-of-view imaged in a single pointing is relatively small (FWHM ~ 17 × λ(mm) arcseconds). Second, in its more extended configurations, the resolution delivered by ALMA can be "too good", running the risk of detecting only compact features, while resolving out the more extended emission.

Thus, to use ALMA as an effective deep sub-mm/mm survey instrument, we actually need to use it in a relatively compact configuration, and to mosaic together several individual ALMA pointings in order to create a homogeneous image of significant size. Nonetheless, this effort is worthwhile, because only ALMA can break through the confusion limit of existing single-dish sub-mm/mm surveys, and enable us to properly connect our ultraviolet (UV)/optical and IR/mm views of the young Universe.

ALMA and the Hubble Ultra Deep Field

As ALMA gradually came on line, the early mosaicing options on offer were understandably limited, with maximum mosaic size initially restricted to 45 pointings. Coincidentally/fortuitously, the size of such an ALMA mosaic, if constructed at mm wavelengths, corresponds closely to the ~ 4.5 square arcminute field of view of the Wide Field Camera 3 (WFC3) instrument on HST, which has recently been used to complete the deepest ever optical-near-infrared image of the sky, the Hubble Ultra Deep Field (HUDF; see, for example, Ellis et al., 2013).

The HUDF was therefore the obvious location for the first deep, blank-field survey with ALMA, and in Cycle 1 we successfully proposed to use 20 hours of ALMA observing time to create a 45-pointing mosaic image of the HUDF at 1.3 mm. This project was, by some margin, the largest project approved in ALMA Cycle 1, and in the end was (understandably) not undertaken until ALMA Cycle 2. However, data taking was finally completed in summer 2015, and we were able to use the data to produce the image shown in Figure 1 (from Dunlop et al., 2016).

In this first ALMA map of the HUDF, the noisy edges of the 45-pointing mosaic can be clearly seen, but it is also apparent that we have succeeded in achieving the desired homogenous coverage of the region previously imaged with the HST. The image shown here has an RMS depth of 35 μJy, and an angular resolution of 0.7 arcseconds (FWHM). It contains 47 > 3.5σ peaks, but source-finding on the inverted (negative) image revealed 29 apparent "sources" down to the same significance level, suggesting that < 20 of the apparent sources in the positive map were real.

Fortunately, the positional accuracy of the ALMA sources, combined with the exquisite depth of the HST imaging (reaching > 30 AB mag), enabled us to isolate the real ALMA sources from the interlopers by looking for counterparts in the HST imaging within a small (< 0.5 arcsecond) search radius. The result of this process is a sample of 16 robust sources. These are marked in Figure 1, and shown in more detail in Figure 2, where contours from the ALMA 1.3 mm imaging are overlaid on colour images created from the optical-near-infrared HST images (*i*+*Y*+*H* bands). As an interesting aside, this ALMA+HST cross-matching revealed that the coordinate system of the HST imaging in the HUDF had to be moved south by ~ 0.25 arcseconds; this offset has been applied in Figure 2 (Dunlop et al., 2016; Rujopakarn et al., 2016).

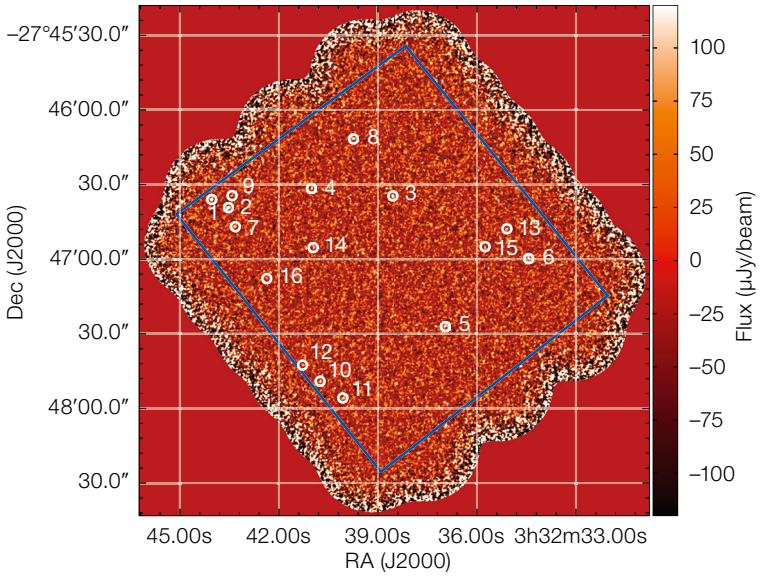

Figure 1. The ALMA 1.3-mm map of the HUDF, with the positions of the 16 detected sources marked by 3.6-arcsecond diameter circles. The border of the homogeneously deep region of near-infrared WFC3/IR HST imaging is indicated by the dark-blue rectangle.

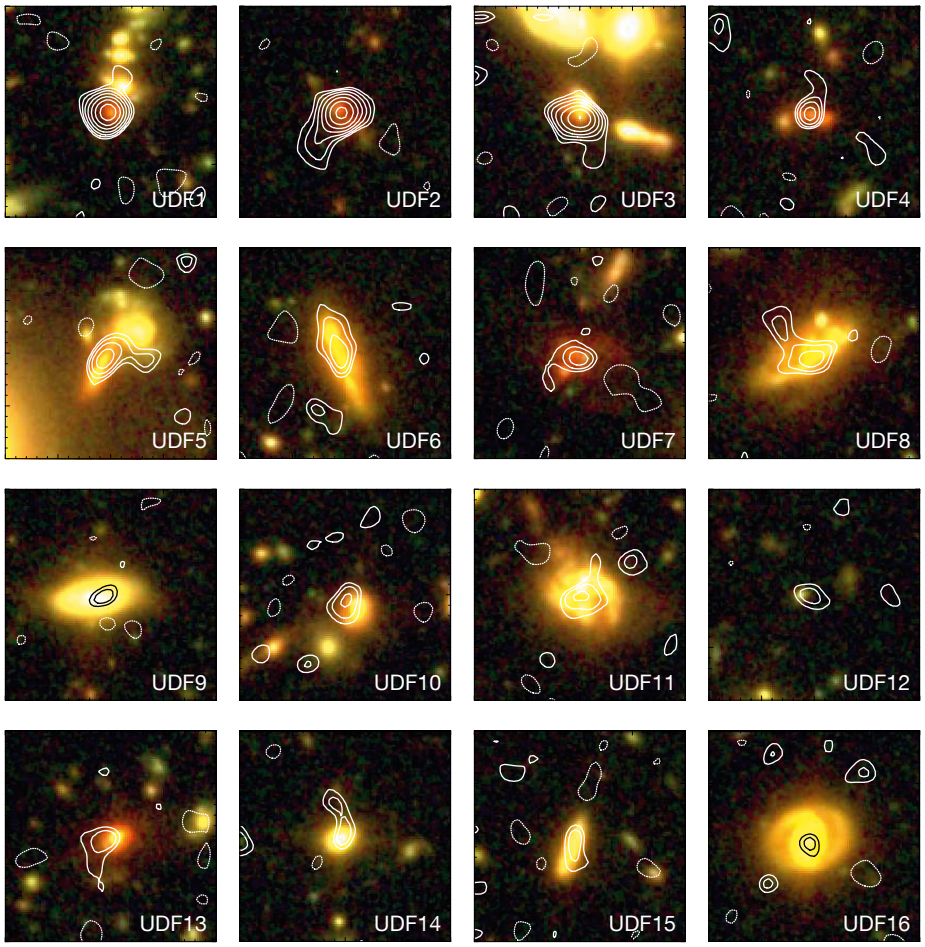

Figure 2. Colour (i_{775} + Y_{105} + H_{160}) HST postage-stamp images of the 16 ALMA detected galaxies in the HUDF, with the contours from the ALMA 1.3-mm imaging overlaid. Each stamp is 6 × 6 arcseconds in size, with north to the top and east to the left.

The nature of the ALMA-detected galaxies

Although we did not quite achieve our desired depth of 30 μJy, this cannot explain the fact that our ALMA-detected sample of 16 sources was substantially smaller than anticipated based on pre-existing estimates of the source counts from other studies (for example, Fujimoto et al., 2016). This finding may mean that the HUDF is somewhat under-dense compared to typical regions of the sky, but it is almost certainly at least partly due to the fact that most previous studies have lacked the quality of supporting data required to separate real from fictitious sources.

Nevertheless, our analysis has revealed that the detected sources form an interestingly homogeneous sample of galaxies. From Figure 2 it can be seen that most are red clumpy galaxies in the HST imaging. Their red colour is partly due to the impact of dust obscuration, but also reflects their redshifts, with 13/16 sources lying in the redshift range $1 < z < 3$. This mirrors the findings of previous studies of brighter sub-mm galaxies, which have generally yielded a median redshift of $z = 2–2.5$.

Aided by the fact that we already know the redshifts and physical properties of the ~ 2000 galaxies previously uncovered by HST in the HUDF, we can explore further the nature of the ALMA-detected sources in the context of the general galaxy population. This is illustrated in Figure 3. In the first panel it can be seen that the ALMA-detected galaxies appear thoroughly unexceptional in terms of UV luminosity (and, hence, raw unobscured star formation rate). However, the true nature of these sources is revealed in the second panel of Figure 3, where it can be seen that they are confined to the high-mass regime. Indeed, in the redshift range $2 < z < 3$, our ALMA image has detected virtually all (7/9) of the galaxies in the field with stellar masses $M_* > 2 \times 10^{10}\ M_\odot$ (assuming a Chabrier (2003) stellar initial mass function [IMF]). Also interesting is the fact that we have detected only one galaxy at $z > 3$, which happens to lie at $z \sim 5$. However, it can also be seen from Figure 3 that the HUDF probes too small a cosmological volume to contain any galaxies with $M_* > 2 \times 10^{10}\ M_\odot$ at $z > 3$, so the absence of higher-redshift sources may simply reflect the evolution of the underlying galaxy mass function.

While many of the physical properties of the ALMA-detected galaxies can be determined from the pre-existing optical-near-infrared data in the HUDF, we need to use the ALMA measurements themselves to estimate the far-infrared luminosities of the sources, and hence their dust-enshrouded star formation rates. Unfortunately this requires some extrapolation from the ALMA flux densities because, for sources at $1 < z < 3$, the peak of the far-infrared spectral energy distribution (SED) lies significantly shortward of the observed wavelength of 1.3 mm (for any reasonable dust temperature). Additional ALMA imaging, reaching down to observed wavelengths of 350 μm, would be helpful in this regard, but for now we must make do with highly uncertain/de-blended Herschel and Spitzer detections/limits for the sources, which span the observed wavelength range 24–500 μm.

In practice, most of our sources are too faint to establish a reliable far-infrared SED for each individual object, and so instead we have created and modeled the typical SED of the objects in our sample by using the available photometry and redshift information to create a pseudo-spectrum. This is shown in Figure 4, where the data have been modeled by a composite source for the purpose of inferring star formation rates from the ALMA photometry. The best-fitting SED shown here has a 20 % (in terms of bolometric luminosity) contribution from an

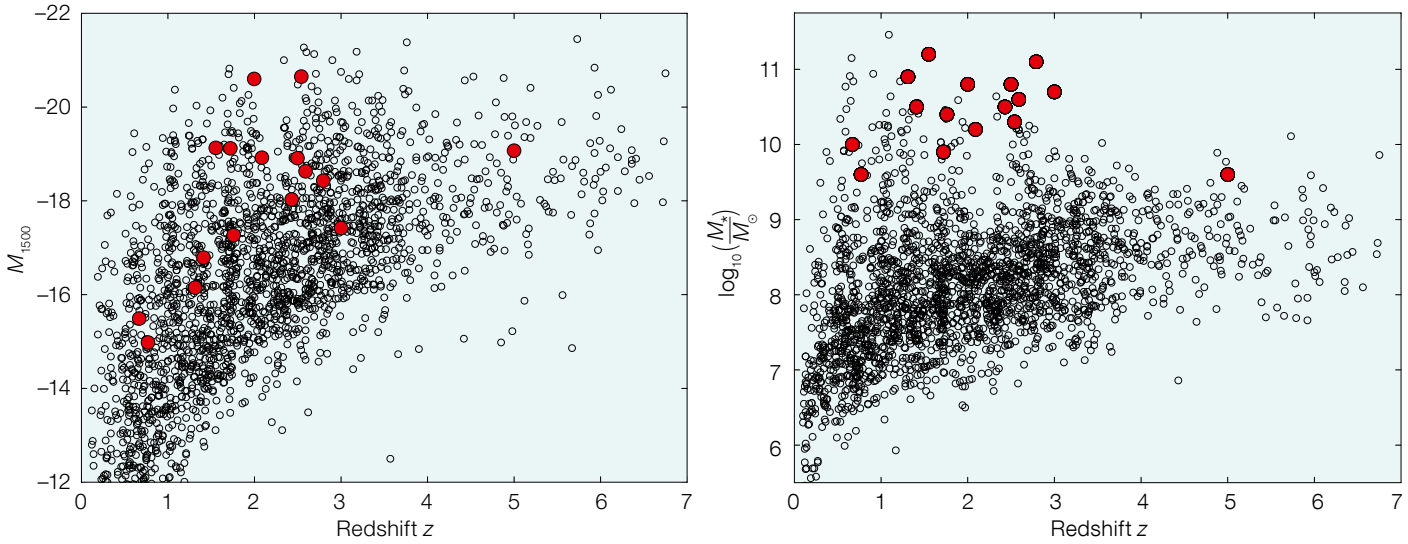

Figure 3. (above) The ALMA sources in the context of the general galaxy population in the Hubble Deep Field. The left panel shows UV absolute magnitude (at λ_{rest} = 150 nm) versus redshift, while the right panel shows the logarithm of stellar mass versus redshift. In both plots the ALMA-detected galaxies are highlighted in red.

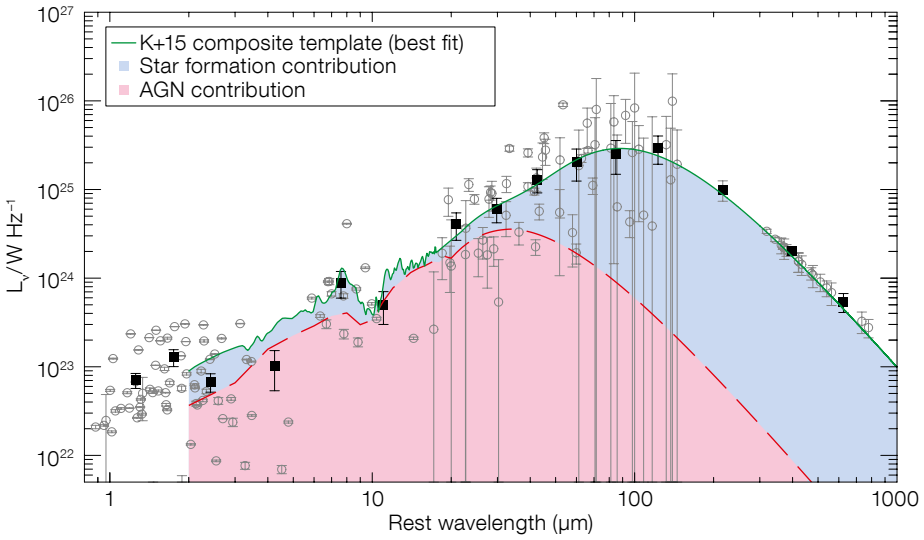

Figure 4. The combined Spitzer+Herschel+ALMA photometry of the 16 ALMA sources, (after de-redshifting and scaling to the same rest-frame 1.3-mm luminosity), fitted by the composite star-forming+AGN template of Kirkpatrick et al. (2015). The solid black squares indicate the weighted mean of the scaled multi-source photometry within a given wavelength bin. The accuracy of the redshift information results in the 8 μm feature being clearly visible in the observed combined rest-frame SED.

AGN, but at longer wavelengths is entirely dominated by dust-obscured star formation (Kirkpatrick et al., 2015). The star formation rates inferred from this SED reveal that our sources have dust-obscured star formation rates ranging from ~ 300 down to ~ 30 $M_\odot$ yr^{-1} (for a Chabrier [2003] IMF).

Astrophysical implications

It is already clear from Figure 3 that stellar mass is a good predictor of a large amount of dust-enshrouded star formation at z ~ 2. However, after calculating the star formation rates as described above, it becomes even clearer that this is the case. If we calculate specific star formation rates (sSFR) by dividing star formation rate by stellar mass, we find that the ALMA-detected objects have, on average, exactly the sSFR expected from the so-called main sequence of star-forming galaxies first discussed by Noeske et al. (2007) and Daddi et al. (2007). Our derived average value of sSFR for the ALMA-detected sources at $1 < z < 3$ is 2.2 Gyr^{-1}, and a stack of the galaxies in the same redshift range and next decade in stellar mass reveals an identical value (see Dunlop et al., 2016). This result favours a simple star-forming main sequence at z ~ 2, with star formation rate proportional to stellar mass out to the highest stellar masses. Interestingly, without the ALMA data, one would infer a flattening of the main sequence at high stellar masses, as has been suggested in several previous studies (for example, Speagle et al., 2014).

It is also apparent that the ratio of dust-obscured to unobscured star formation is a steep function of stellar mass, apparently increasing by a factor of about 10 between M_* ~ 3 × 10^9 $M_\odot$ and M_* ~ 3 × 10^{10} $M_\odot$. Together, these two factors combine to produce a very strong dependence of ALMA detectability on stellar mass (proportional to ~ M_*^2), with the result that the detectability of galaxies at sub-mm/mm wavelengths drops off very rapidly below M_* ~ 10^{10} $M_\odot$.

Cosmic star formation history

Finally, we can use these results to derive the evolution of the co-moving UV luminosity density and the co-moving

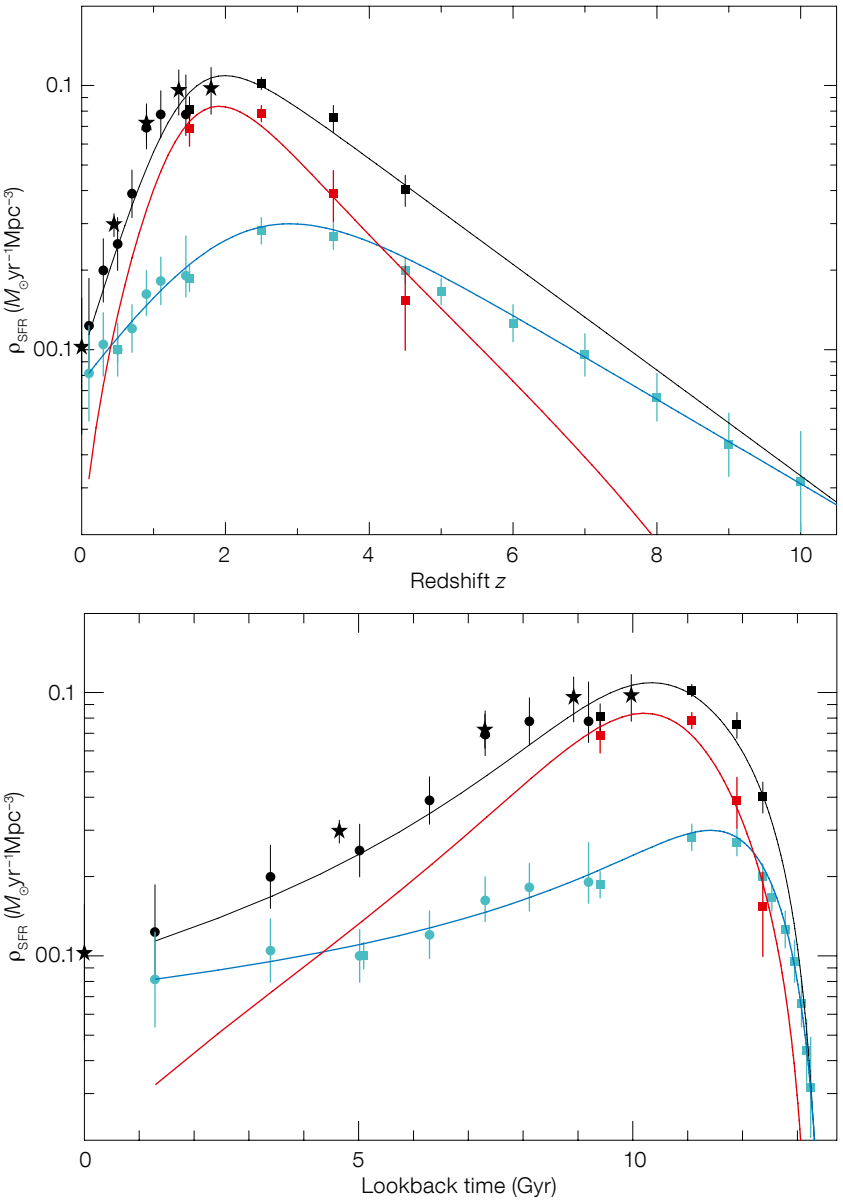

Figure 5. The evolution of co-moving star formation rate density (ρ_{SFR}) as a function of redshift (upper panel) and cosmic time (lower panel). The blue points and blue (double power-law) fitted curve show the raw, unobscured UV-derived values of ρ_{SFR} (derived from: Cucciati et al., 2012; Parsa et al., 2016; McLure et al., 2013; and McLeod et al., 2015). The red points and curve indicate the dust-obscured estimates of ρ_{SFR} derived from the present ALMA study of the HUDF (Dunlop et al., 2016). The black points and curve show total ρ_{SFR}; at $z < 2$ the data are from Cucciati et al. (2012) and Burgarella et al. (2013), while at $z > 2$ the black data points are simply the sum of the blue (unobscured) and red (dust-obscured) values.

far-infrared luminosity density as a function of redshift, converting the luminosity densities to visible and obscured star formation rate densities respectively (see Kennicutt & Evans, 2012).

Our knowledge of the evolution of the cosmic star formation rate density following the first results from WFC3+HST and Herschel (both of which came into operation in 2009) was reviewed by Behroozi et al. (2013) and Madau & Dickinson (2014). However, the deeper census of dust-obscured star formation enabled by the new ALMA results allows us to better determine the relative evolution of obscured and unobscured star formation at redshifts z = 2–5. The implications of our new results are summarised in Figure 5. The upper panel shows the evolution of unobscured, obscured and resulting total star formation rate density as a function of redshift, with the lower panel simply showing the equivalent information as a function of cosmic time. Now it can be seen clearly that, while the star formation density around the peak epoch at z = 2–2.5 is overwhelmingly dominated by dust-obscured emission from massive galaxies, at redshifts higher than z ~ 4 the dust-obscured component drops off rapidly, with the consequence that the star-forming Universe is primarily unobscured at earlier times (i.e., within 1.5 Gyr of the Big Bang).

Deeper imaging (for example, Walter et al., 2016) and wider-area surveys with ALMA have the potential to clarify this behaviour still further, and in particular to determine the evolution of dust-obscured star formation activity as a function of redshift at fixed galaxy stellar mass. In addition, the sources uncovered by these deep ALMA surveys are obvious attractive targets for further ALMA pointed imaging+spectroscopy extending to shorter wavelengths, and for future study with the James Webb Space Telescope (JWST).

References

Behroozi, P. S., Wechsler, R. H. & Conroy, C. 2013, ApJ, 770, 57
Bourne, N. et al. 2016, arXiv:1607.04283
Burgarella, D. et al. 2013, A&A, 554, 70
Chabrier, G. 2003, PASP, 115, 763
Coppin, K. E. K. et al. 2006, MNRAS, 372, 1621
Cucciati, O. et al. 2012, A&A, 539, 31
Daddi, E. et al. 2007, ApJ, 670, 156
Dunlop, J. S. et al. 2016, MNRAS, in press, arXiv:1606.00227
Ellis, R. S. et al. 2013, ApJ, 763, L7
Fujimoto, S. et al. 2016, ApJS, 222, 1
Geach, J. E. et al. 2013, MNRAS, 432, 53
Hughes, D. H. et al. 1998, Nature, 394, 241
Kennicutt, R. C. & Evans, N. J. 2012, ARA&A, 50, 531
Kirkpatrick, A. et al. 2015, ApJ, 814, 9
Madau, P. & Dickinson, M. 2014, ARA&A, 52, 415
McLeod, D. J. et al. 2015, MNRAS, 450, 3032
McLure, R. J. et al. 2013, MNRAS, 432, 2696
Michalowski, M. J. et al. 2016, arXiv:1610.02409
Narayanan, D. et al. 2015, Nature, 525, 496
Noeske, K. G. et al. 2007, ApJ, 660, L43
Parsa, S. et al. 2016, MNRAS, 456, 3194
Rujopakarn, W. et al. 2016, arXiv:1607.07710
Speagle, J. S. et al. 2014, ApJS, 214, 15
Walter, F. et al. 2016, ApJ, in press, arXiv:1607.06768
Weiss, A. et al. 2009, ApJ, 707, 1201